Journal of Neuroscience Methods 406 (2024) 110131

Contents lists available at ScienceDirect

Journal of Neuroscience Methods

journal homepage: www.elsevier.com/locate/jneumeth

Concurrent spinal and brain imaging with optically pumped magnetometers

Lydia C. Mardell [a,*], Meaghan E. Spedden [b], George C. O'Neill [b], Tim M. Tierney [b], Ryan C. Timms [b], Catharina Zich [a], Gareth R. Barnes [b], Sven Bestmann [a,b]

[a] Department of Clinical and Movement Neurosciences, UCL Queen Square Institute of Neurology, University College London, WC1N 3BG, UK
[b] Wellcome Centre for Human Neuroimaging, Department of Imaging Neuroscience, UCL Queen Square Institute of Neurology, University College London, WC1N 3AR, UK

ARTICLE INFO

Keywords:
Wearable MEG
Cortico-spinal interactions
Spinal cord
Magnetospinoencephalography

ABSTRACT

Background: The spinal cord and its interactions with the brain are fundamental for movement control and somatosensation. However, brain and spinal electrophysiology in humans have largely been treated as distinct enterprises, in part due to the relative inaccessibility of the spinal cord. Consequently, there is a dearth of knowledge on human spinal electrophysiology, including the multiple pathologies that affect the spinal cord as well as the brain.

New method: Here we exploit recent advances in the development of wearable optically pumped magnetometers (OPMs) which can be flexibly arranged to provide coverage of both the spinal cord and the brain in relatively unconstrained environments. This system for magnetospinoencephalography (MSEG) measures both spinal and cortical signals simultaneously by employing custom-made scanning casts.

Results: We evidence the utility of such a system by recording spinal and cortical evoked responses to median nerve stimulation at the wrist. MSEG revealed early (10 – 15 ms) and late (>20 ms) responses at the spinal cord, in addition to typical cortical evoked responses (i.e., N20).

Comparison with existing methods: Early spinal evoked responses detected were in line with conventional somatosensory evoked potential recordings.

Conclusion: This MSEG system demonstrates the novel ability for concurrent non-invasive millisecond imaging of brain and spinal cord.

1. Introduction

The spinal cord transmits sensory information from the periphery to the brain and constitutes the final stage of processing within the central nervous system (CNS) for the production of movement. Yet in humans, it is also one of the most difficult structures of the central nervous system to study (Giove et al., 2004; Filli and Schwab, 2012; Stroman et al., 2014; Dauleac et al., 2020).

One fundamental barrier to our understanding of human spinal cord function in health and disease is the limited ability to study its electrophysiology, due to the inaccessibility of the spinal cord (Stroman et al., 2014). The limitations to study the spinal cord with both high spatial and temporal resolution have led to a poor understanding of the functional neuropathology of the spinal cord and cortico-spinal interactions.

Consequently, there is an unmet need for spinal imaging with millisecond precision because many acquired and neurodegenerative diseases that act on the brain also affect the spinal cord, and vice versa (Furby et al., 2008; Freund et al., 2012; Grabher et al., 2015; Panara et al., 2019). For example, acute and chronic pain provoke both spinal and cortical changes (Moore et al., 2002; Baliki et al., 2011; Sprenger et al., 2015), damage to the spinal cord from spinal cord injury leads to profound retrograde degeneration (Grabher et al., 2015), and damage to the brain after stroke can result in anterograde changes at the spinal level (Lamy et al., 2009; Karbasforoushan et al., 2019).

One implication is that our understanding of many neurological disorders remains incomplete in terms of their spinal mechanisms, and development of novel treatment approaches or rehabilitation regimes often overlook the role of the spinal cord or rely on small animal disease models (Filli and Schwab, 2012).

Development of electrophysiological imaging of the human spinal

* Corresponding author.
E-mail address: Lydia.mardell.17@ucl.ac.uk (L.C. Mardell).

https://doi.org/10.1016/j.jneumeth.2024.110131
Received 18 August 2023; Received in revised form 11 March 2024; Accepted 3 April 2024
Available online 5 April 2024

cord, concurrently with imaging of the brain, will thus be foundational to deeper understanding of the spinal cord in health and disease.

1.1. Current measures of spinal activity

Direct spinal physiology is difficult to study in humans. Corticospinal activity has been largely inferred via indirect measures such as cortico-muscular coherence and transcranial magnetic stimulation (TMS) (Keil et al., 2014; Derosiere et al., 2020; Ibáñez et al., 2021). These techniques rely on activating or recording from the cortex and/or muscles, and generally assess the specific contribution of the spinal cord indirectly. Furthermore, interactions between brain and spinal cord are difficult to untangle from influences of either region.

Advances in functional magnetic resonance imaging (fMRI) can quantify cortical and spinal interactions in humans, although not without challenges (see Kinany et al. 2022 for a review). For example, combined brain-spinal cord fMRI has identified resting brain-spinal networks (Vahdat et al., 2020), which are compromised following disease (Landelle et al., 2023). One advantage of electrophysiological imaging of the spinal cord is the higher temporal precision that can complement the higher spatial precision afforded by fMRI.

The literature on precise recordings of human spinal electrophysiology, however, remains dominated by direct, invasive measurements, often recorded during surgery (Urasaki et al., 1990; Prestor et al., 1991; Imajo et al., 2021). Commonly used non-invasive techniques for measuring spinal electrophysiology generally rely on surface electrodes, which, for example, can detect spinal cord evoked potentials (SCEPs) following electrical stimulation of peripheral nerves (Cracco, 1973; Iragui, 1984; Restuccia et al., 1994; Fujimoto et al., 2001). Peripheral nerves, such as the median and ulnar nerves of the upper limb, are mixed nerves that can be non-invasively stimulated to evoke somatosensory potentials. N9, the peripheral volley, which is a compound action potential generated by mixed nerve stimulation, is easily detected as it is a mixture of orthodromic (i.e., physiologic direction) and antidromic (i.e., against physiologic direction) responses. The postsynaptic dorsal horn volley, N13, is best recorded over the posterior neck between C6 – C7 spinous processes. Both potentials are commonly used clinical measures for diagnostics (Urasaki et al., 1990; Restuccia et al., 1994; De Oliveira et al., 2022).

Excitingly, the dearth of ways to study spinal cord electrophysiology in humans have recently spawned several novel developments. For example, high-density, multi-channel electrode montages with spatial filtering improve the sensitivity such that spinal cord evoked potentials (SCEPs) can be detected at the single-trial level (Nierula et al., 2022). This approach, combined with peripheral nerve action potentials and somatosensory evoked potentials (SEPs) at the level of the brainstem, enables the assessment of the electrophysiological bottom-up signal integration. Further, Chander and colleagues have recently shown that high frequency signals (200 – 1200 Hz) can be detected at the cervical spinal level with surface electrodes surrounding the neck, at latencies between 8 – 16 ms after median nerve stimulation (Chander et al., 2022). Recordings using surface electrodes can therefore provide insights into the top-down and bottom-up dynamics of the human spinal cord.

In addition to techniques measuring electrical spinal activity, the magnetic field generated can be measured using superconducting quantum interference devices (SQUIDs). One advantage, compared to surface-based electrodes, is their relative insensitivity to the distortion of the volume currents caused to surrounding tissue which traditionally limits precise estimates of the underlying sources (Akaza et al., 2021). This has motivated the development of magnetospinography (MSG) (Adachi et al., 2013; Kawabata et al., 2002; Sakaki et al., 2020; Sumiya et al., 2017; Ushio et al., 2019). The magnetic fields detected with MSG are not as distorted by the tissue surrounding the spinal cord, an advantage for source analyses (Kawabata et al., 2002). Although MSG is by no means immune to muscle artefacts, reduced muscle interference provides a benefit over electrode-based recordings (Claus et al., 2012; Muthukumaraswamy, 2013; Boto et al., 2019).

Recent MSG systems are based upon custom-built arrays of SQUID sensors within rigid cryogenic vessels (dewars) filled with liquid helium (Akaza et al., 2021). Both reclining and supine position scanning systems have been developed, optimized to record from the cervical spine (Miyano et al., 2020; Sumiya et al., 2017). These systems allow the detection of magnetic fields generated by spinal neurons and innervating nerves, including early spinal cord evoked fields (SCEFs) following supramaximal peripheral nerve stimulation (Akaza et al., 2021; Miyano et al., 2020).

MSG offers a unique way to capitalize on the benefits of SQUID-based imaging of the spinal cord. However, it also requires the participant to remain still, in a rigid upright or supine position (Sumiya et al., 2017), making studies of spinal cord electrophysiology during movement, or studies of patient cohorts that have difficulty staying immobile, challenging. The coverage of the spinal cord is furthermore dictated by the size and shape of the specific fixed SQUID array, rather than being fit to the subject's anatomy and adapted to the specific question at hand, such as imaging the cervical versus lumbar spinal cord. Finally, these systems currently cannot record simultaneously from the brain and spinal cord, preventing the study of interactions between the two areas.

1.2. Magnetospinoencephalography (MSEG) with optically pumped magnetometers

Here we present a novel system for concurrent spinal and brain recording with millisecond precision. To this end, we leverage the development of wearable magnetoencephalography (MEG) systems (Boto et al., 2018; Seymour et al., 2021; Brookes et al., 2022) incorporating optically pumped magnetometers (OPMs). OPMs are sensing devices that can measure the absolute magnetic field changes caused by neuronal current flow, which were previously commonly recorded with large, inflexible superconducting systems (Tierney et al., 2019). Recent progress in miniaturization and commercialization now provides access to OPMs that are lightweight and small (12.4 × 16.6 × 24.4 mm), approximately the size of a 2 × 4 LEGO brick. Usually, these sensors are placed in a helmet that can be worn by the participant (Boto et al., 2017; Hill et al., 2019; Roberts et al., 2019; Seymour et al., 2021). In contrast to traditional SQUID-based MEG systems, which comprise a rigid superconducting flask, the field-sensitive volume of the device can be placed flexibly within 6 – 8 mm of the skin surface. By reducing the distance between the source and the sensors, the signal can be amplified by a factor equal to the inverse square of the distance, which results in an improvement in spatial resolution (Boto et al., 2016; Iivanainen et al., 2017). Flexible sensor placement and wearability of OPM-based MEG (OP-MEG) has enabled detection of neuromagnetic fields generated by deep sources such as the cerebellum (Lin et al., 2019) and hippocampus (Barry et al., 2019; Tierney et al., 2021b). OPMs thus provide the perfect building blocks for a novel magnetospinoencephalographic (MSEG) approach to capture neuromagnetic field changes from deep spinal sources and the brain concurrently.

Leveraging these developments in OP-MEG, we have developed a flexible MSEG system that allows for recording concurrent spinal and cortical electrophysiology. Here we report early and late evoked fields over the cervical spine, in combination with cortical sensory evoked fields, in response to median nerve stimulation at the wrist. This provides a first demonstration for the feasibility of spinal imaging using OPMs, concurrently with the brain. With this proof-of-principle demonstration for wearable MSEG, one can now capitalize on the rapid developments in OPM imaging for studying cortico-spinal mechanism of somatosensation and action in health and disease.

2. Methods

2.1. Participant information

This study was approved by the University College London research ethics committee and conducted in line with the *Declaration of Helsinki*, except for pre-registration in a database prior to study recruitment. Two healthy male participants (participant A, aged 45; participant B, aged 55) took part in the present study after providing informed written consent. Participant A underwent one SEP session and five OPM sessions (OPM sessions 2 and 3 took place on consecutive days, 1 month after session 1, session 4 and 5 respectively occurred 7 and 19 months after session 1). Participant B took part in one SEP session and one OPM session.

2.2. Clinical SEP recordings

Spinal and cortical SEPs were recorded, using a standard clinical set-up, to compare peak latencies with evoked fields. To this end, Ag-AgCl cup electrodes were placed on ipsilateral Erb's point, between the C6 and C7 spinous processes (Cv7) and on the scalp over the contralateral cortical sensorimotor area (C3) with conductive paste and secured with tape. Electrodes were referenced to Fz and the ground was placed on Cz. Data were sampled at 1280 Hz with a 3 Hz high pass filter and 3 kHz low pass filter. The right median nerve was stimulated at the wrist with a pulse width of 200 μs and stimulation rate of 3.11 Hz. The stimulation intensity was identified by increasing it until a reproducible muscle twitch occurred without participant discomfort. Responses were averaged over 200 trials.

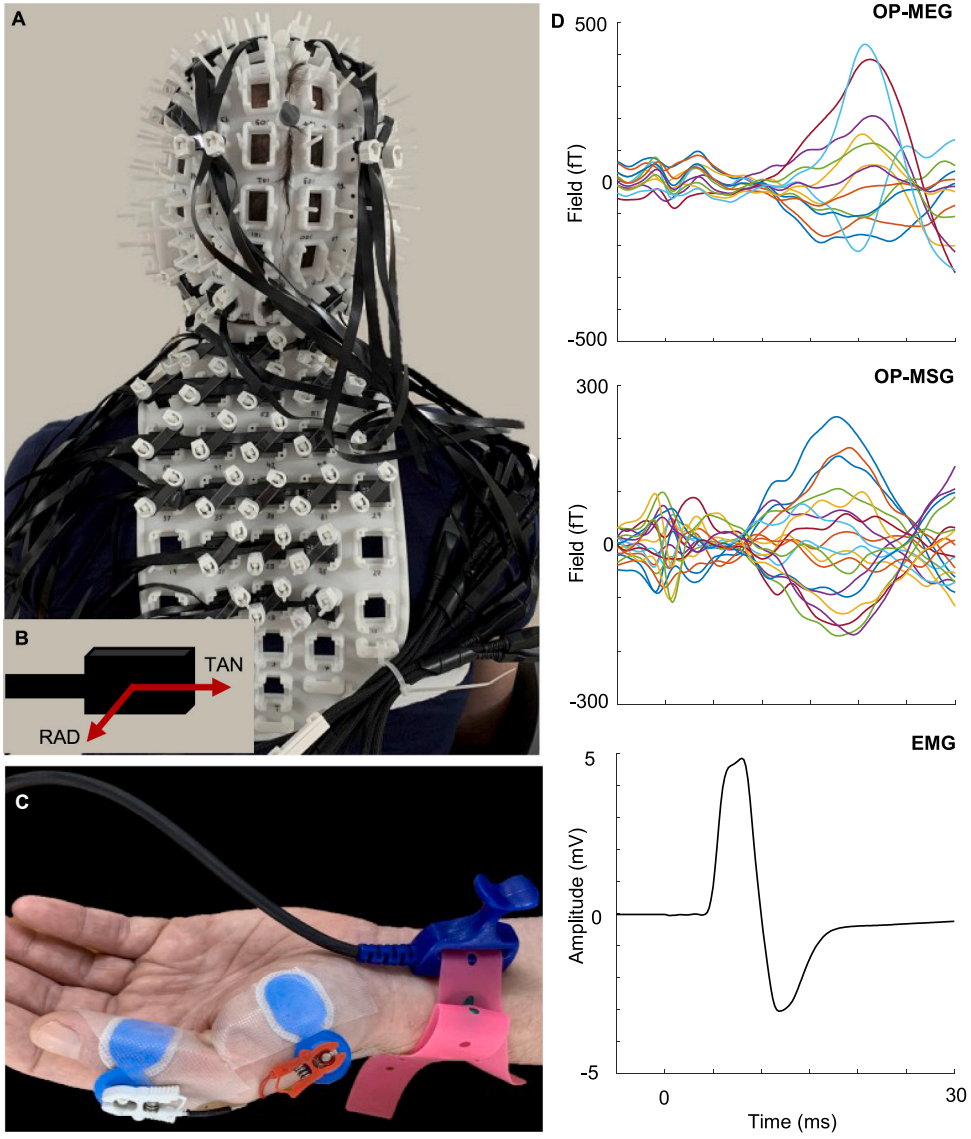

Fig. 1. Experimental setup for participant A. **A.** 3D printed customized spinal- and head-cast. The head-cast contains optically pumped magnetometer (OPM) sensors over the base of the head and sensorimotor cortex. During the recording the subject is seated on a wooden stool within the magnetically shielded room. **B.** Schematic of OPM sensor, demonstrating the two axes: radial (RAD) and tangential (TAN) to the spinal cord and cortex. **C.** Median nerve stimulation (MNS) electrode applied to the wrist with electromyography (EMG) electrodes recording the abductor pollicis brevis (APB) muscle activity. **D.** Example activity across the nervous system in response to right wrist MNS for participant A during session 5 (averaged over 2260 trials). From top to bottom: OPM-based magnetoencephalography (OP-MEG) from the left cortical region; OPM-based magnetospinography (OP-MSG); EMG of APB muscle.

2.3. SEP data analysis

Averaged SEPs were cropped from 1 ms onwards, to remove the stimulation artefact, and converted to FieldTrip format. Data were bandpass filtered between 20 – 300 Hz to derive time courses comparable to the OPM data. Peak latencies for N9, N13 and N20 were extracted from Erb's point, Cv7 and C3 time courses, respectively.

2.4. OPM scanner cast design

Both participants had unique spinal scanner casts developed, customized to their body shape. An optical white light scanner was used to generate a 3D model of participant A's upper body for which the spinal OPM scanner cast was created (Chalk Studios, London, UK). The spinal scanner cast, providing coverage of the neck and back, was 3D printed in nylon with Velcro straps attached to hold the cast in place during scanning (Fig. 1A). The spinal scanner cast contains a total of 33 OPM sensor slots, of which a maximum of 27 slots were utilized in the current study. For the cortical sensor array, a personalised head-cast constructed from the individual's structural MRI scan (Chalk Studios, London, UK) was used to capture the magnetic field over the contralateral sensorimotor cortex.

The spinal OPM scanner cast for participant B was based on a 3D upper body model constructed using a Structure sensor (optical camera) mounted on an iPad running Skanect software. This cast was also 3D printed (Chalk Studios, London, UK) and contained a total of 41 sensor slots. The slots covered the lower neck and upper back, as well as the front of the shoulder, around the clavicle.

2.5. OPM data acquisition

All data were recorded in a magnetically shielded room (MSR), with internal dimensions of 438 × 338 × 218 cm, which included several design optimizations to improve magnetic shielding (Magnetic Shields Ltd, Staplehurst, UK). The room comprises of two inner layers of 1 mm mu-metal, a 6 mm copper layer and two external layers of 1.5 mm mu-metal. Prior to each scanning session, magnetic equilibration of the MSR was achieved through a process known as degaussing. This involves applying a sinusoidal current, which decreases in a stepwise fashion, to coils wound around the shielding material, inducing a magnetic flux in a closed loop (Altarev et al., 2015). Automated sensor-level nulling with inbuilt field cancellation coils prior to every experimental recording further reduces residual fields around the vapour cell of the OPM sensors (Osborne et al., 2018; Seymour et al., 2021).

Data were recorded from the QuSpin OPM sensors (QuSpin Inc., Louisville, USA) at a sampling rate of 6 kHz and saved in brain imaging data structure (BIDS) format. The OPM sensors have a sensitivity of ~15 $fT/\sqrt{Hz}$ between 10 and 100 Hz (Boto et al., 2022), measurements up to 500 Hz are still possible but with reduced sensitivity (Bu et al., 2022).

In the first four sessions for participant A, two reference dual-axis OPM sensors were placed 1 – 2 m away from the participant, in fixed positions within the MSR, to capture the environmental magnetic field changes. Reference sensors were not used in the session 5 nor for participant B as the benefit of additional physiological sensors was deemed greater than benefit reference sensors provide.

Participant A underwent five separate OPM recording sessions seated in the centre of the MSR. An array consisting of 21, 27, 27, 24 and 19 dual-axis OPM sensors in session 1 – 5 respectively were arranged in the custom-made spinal scanner cast to cover the neck and upper back. Variability in sensor number was due to sensor availability at the time of recording and differences in sensor arrangement occurred at the edges of the array to ensure the cervical spinal cord was always well covered. In addition to the spinal coverage, session 5 also comprised cortical recording from 13 OPM sensors that were arranged over the sensorimotor cortex in a customized 3D printed OPM head-cast (Fig. 1A).

Participant B completed one recording session with 26 triaxial OPM sensors (78 channels) arranged over the upper back and shoulders. Participant B was in the prone position during the recording to maximise relaxation of the back muscles. Here we use the term 'sensor' to refer to the physical device and the term 'channel' to refer to the oriented axis within the sensor. Differences in acquisition parameters across sessions reflect the fast development in the field.

2.6. Median nerve stimulation (MNS)

During the OPM recordings, the median nerve was stimulated at the wrist via a peripheral nerve stimulation electrode with the anode positioned distally to the cathode (Fig. 1C). We chose median nerve stimulation (MNS) to probe the CNS, due to the time-locked nature of the expected response and the wealth of previous literature providing strong priors about the latency of the evoked field (Akaza et al., 2021; Cracco, 1973; Jones, 1977; Mizutani and Kuriki, 1986). Pulses were delivered with a 50 μs pulse-width at a stimulation frequency of 2 Hz using a DS7A current stimulator (Digitimer Ltd, Hertfordshire, UK). A total of 565 stimulations were delivered for each run with a short break between runs. For all sessions, stimulation was suprathreshold to induce a reliable thumb twitch (stimulator intensity 12 – 31.2 mA). For participant A, session 1 and session 2 consisted of four runs of right MNS (a total of 2260 trials). Session 3 consisted of two runs of each right and left MNS (1130 per wrist) and session 4 consisted of nine runs of left MNS (3 ×1695 trials), see Section 2.8 for further details.

Recordings for session 5 and participant B included four runs of right MNS, each consisting of 565 stimulation trials and 10 – 20 drop trials (randomly spread throughout), where the stimulation was omitted. The participant was asked to count the number of drop trials and report this to the experimenter at the end of each run to ensure the participant was attending to the stimulation. The cognitive task was included to prevent the participants from tiring and to keep levels of attention constant. The present study's primary focus was on the evoked (short latency) responses, which are not influenced by changes in attention (Desmedt et al., 1983; García-Larrea et al., 1991), and differences between sessions are therefore unlikely to be caused by the inclusion of this task.

2.7. EMG recording

During session 5 for participant A, surface electrodes were used to record electromyography (EMG) of the abductor pollicis brevis (APB) muscle twitch. Data were recorded at a sampling frequency of 5 kHz, with a high pass filter at 3 Hz and low pass filter at 1000 Hz.

2.8. Varying median nerve stimulation intensity

In all recordings, suprathreshold MNS was used to elicit a reliable thumb twitch. For all sessions, excluding session 4, stimulation intensity was identified by finding a reproducible thumb twitch and then increasing the strength of the stimulation to the maximum intensity that the participant was comfortable with. During session 4 for participant A, to assess the impact of stimulation intensity on spinal evoked fields the stimulation intensity was set to motor threshold (MT), 1.5 x MT and 2.5 x MT. Three runs of 565 trials were recorded at each intensity, resulting in a total of 1695 runs each.

2.9. Control experiment

Median nerve stimulation can elicit late, excitatory reflex responses in the trapezius muscle (Alexander and Harrison, 2003; Tataroglu et al., 2011) which may contribute to the OPM signals seen at longer latencies. We therefore assessed the response of upper and lower trapezius fibres to MNS in a separate session, in the same participants. The median nerve was stimulated at the right wrist, with a pulse-width of 1 ms and stimulation frequency of 0.25 Hz (Digitimer DS7A stimulator). Intensities were set to evoke clear, average responses in the trapezius muscles

ipsilateral to the stimulation. This intensity corresponded to 3 and 2 times the MT in the APB muscle for participants A and B, respectively.

Ambu Neuroline 700 surface electrodes (Ambu Ltd, Ballerup, Denmark) were positioned above the ipsilateral lower trapezius fibres medial to the line from the end of the scapular spine to T12. For the ipsilateral upper trapezius, electrodes were positioned midway along the line from C7 to the acromion. Electrodes were positioned with 2 cm interelectrode distance in line with the direction of the muscle fibres. The ground electrode was fastened around the left wrist (Alexander and Harrison, 2002, 2003). EMG signals were acquired using the D360 Amplifier (Digitimer Ltd, Hertfordshire, UK) and 1401 data acquisition unit (Cambridge Electronic Design, UK) and recorded using Spike2 software (v10.05).

MNS was performed both during rest and contraction of the trapezius, where the subjects were seated in a reclining chair and instructed to lift their right arm diagonally in front of them to a position slightly under 90 degrees (Alexander and Harrison, 2003; Tataroglu et al., 2011). 80 trials were recorded from each participant in each condition. EMG signals were mean-centred and low-pass filtered at 200 Hz using a 2nd order Butterworth filter. A student's T-Test was used to calculate T-values for each EMG channel from −20 to +100 ms around stimulation, for each participant and condition.

2.10. OPM data pre-processing

The OPM BIDS formatted data were loaded into SPM format and filtered using homogenous field correction (Tierney et al., 2021a). A 2nd order bidirectional Butterworth bandpass filter between 20 – 300 Hz was used to remove low and high frequency noise. In session 1 – 4 for participant A, where reference sensors were used, synthetic gradiometry was conducted in order to reduce external noise (Fife et al., 1999). Here, the linear regression of the two reference sensors was subtracted from the spinal and cortical sensor data. Synthetic gradiometry was additionally done with narrow-band reference sensor data, bandpass filtered between both 47 – 53 Hz and 97 – 103 Hz, to reduce line noise. Although synthetic gradiometry provided some added benefit in noise reduction, this stage was removed in later recordings (for participant A session 5 and for participant B), to enable use of the additional sensors in the SCEF recording. Individual trials were epoched from −100 to +300 ms around stimulus onset and baseline corrected to the average signal between −100 to 0 ms. Trials from subsequent runs of the same task within sessions were merged and averaged.

2.11. Source localization

Source localization was used to further interrogate later spinal responses witnessed in participant A over multiple sessions. Equivalent current dipole (ECD) fitting was used on data from Participant A to find the optimal dipole location and orientation for the waveform centered ~58 ms, using FieldTrip software (Oostenveld et al., 2011). A window of 52 – 60 ms was used to average the response, in line with the central peak of the spinal 43–58–89 ms complex evoked following wrist MNS, as previously described by Mizutani and Kuriki (1986). Right MNS SCEFs from session 1 – 3 and 5, and left MNS SCEF from session 3, the 1.5 x MT and the 2.5 x MT conditions from session 4 were used for source analysis. The trial averaged SCEFs were averaged in the 52 – 60 ms window before dipole fitting was separately completed for each session.

To produce a volume conductor model, the optical 3D scan, used to generate the spinal scanner cast, was converted into a mesh. The arms and head were removed to produce an empty torso single shell model used for the forward model (Nolte, 2003). A cylinder (diameter 40 mm), within the upper back of the torso model, was used to approximate the location of the spinal cord. This cylinder was the starting point of a non-linear search constrained within the torso model. This identified the optimal coordinate and orientation of the 52 – 60 ms dipole.

2.12. Statistics

T-statistics were computed for the SCEF from all sessions, independently. A student's T-Test was calculated on the SCEF time course, from −10 to +100 ms around stimulation, for all spinal channels (all sensor orientations). The window of −10 to +100 ms around stimulation was chosen to incorporate the early (~10 ms) and later (~45 – 70 ms) responses visualized in the SCEF. The false discovery critical height threshold was calculated using the `spm_uc_FDR` function to correct for multiple comparisons. For this, the false discovery rate was set to 0.05.

2.13. Software

All data and statistical analysis were conducted in MATLAB R2020b (Mathworks Inc., Natick, MA, USA) using the FieldTrip (Oostenveld et al., 2011) and Statistical Parametric Mapping (SPM; https://www.fil.ion.ucl.ac.uk/spm/) toolboxes.

3. Results

3.1. Concurrent brain, spinal cord, and muscle recordings

OPM sensors uniquely allow for non-invasive imaging of the brain and spinal cord simultaneously, facilitating electrophysiology recording over the entire human central nervous system (CNS; Fig. 1). We recorded SCEFs, in response to MNS, in 2 participants (A and B). We built two individual spinal casts optimized to participant A and B. In participant A we measured simultaneously from the spinal cord and cortex. In participant B we measured SCEFs alone.

In addition to brain and spinal cord electrophysiology, for participant A during session 5, we recorded EMG from the abductor pollicis brevis muscle, capturing the activity at each level of the hierarchy of the nervous system (Fig. 1D). The EMG responses to MNS at the wrist had an onset of 4 ms and peaked 6 – 8 ms post stimulation. In this session we found that the greatest response in spinal global field power (GFP; standard deviation over all spinal OPM channels) was the 10 – 15 ms early response, with additional later SCEFs occurring from 20 ms onwards. Simultaneous cortical evoked fields had an initial global field power peak at 21 ms followed by a 30 ms peak, characteristic of cortical MNS evoked response (Allison et al., 1991; Kakigi, 1994).

3.2. Spinal cord evoked potentials and fields in response to median nerve stimulation are comparable

First we compared latencies of SEPs acquired using a standard clinical set-up with latencies of the GFP obtained from OP-MSG. For participant A, peak SEP latencies in response to right MNS occurred at 11 ms at Erb's point (N9) and 15 ms at Cv7 (N13), as shown in Fig. 2Ai. Cortical SEPs peaked at 20 ms (N20), 25 ms and 35 ms (Fig. 2Aii). For participant B, peak SEP latencies occurred at 9 ms at Erb's point (N9) and 15 ms at Cv7 (N13), illustrated by Fig. 2B. Previous MSG studies have found evoked spinal responses to MNS at the wrist occurring 9.7 ms after stimulation (Akaza et al., 2021). As demonstrated by Fig. 2, SEP latencies are comparable to the peak early spinal GFP latencies that we recorded using OP-MSG in response to high suprathreshold MNS for participant A (Fig. 2 Ai) and participant B (Fig. 2B).

Early SCEFs at the expected latency ~10 ms were not present in all recordings. Optimising the study set up, including increased stimulation intensity, along with variability in noise are likely responsible for the presence/absence of this early signal. Sessions where early SCEFs were detected are shown for left and right MNS for participant A (Fig. 3 and Fig. 2A, respectively) and for right MNS in participant B (Fig. 2B).

Peak early (<20 ms) latencies in the SCEF were calculated using absolute maximum T-values, across all spinal channels, that crossed the false discovery rate (FDR) threshold. For participant A peaks occurred at 11 and 16 ms for left MNS (session 4) and 17 ms right MNS (session 5).

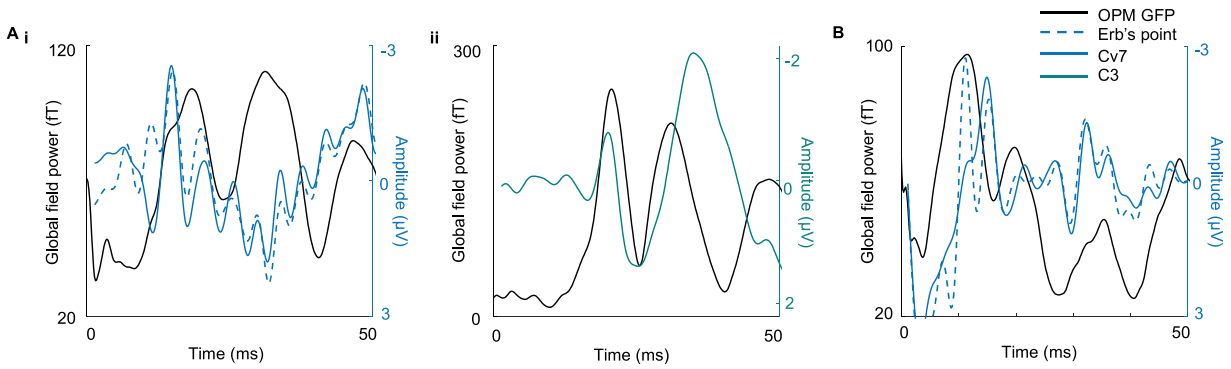

Fig. 2. Comparison of spinal cord evoked potentials and fields. **Ai.** Participant A's global field power (GFP) for all spinal OPM sensors, illustrating key latencies of the spinal cord evoked field (SCEF; black solid line). Overlayed are the somatosensory evoked potentials (SEPs) for the electrode at Erb's point (blue dashed line) and Cv7 (blue solid line). **ii.** Participant A's GFP for all cortical OPM sensors (black solid line) with the cortical SEP from C3 overlayed. **B**. As in Ai but for participant B. Vertical black dotted lines represent every 10 ms from 10 – 40 ms post stimulation.

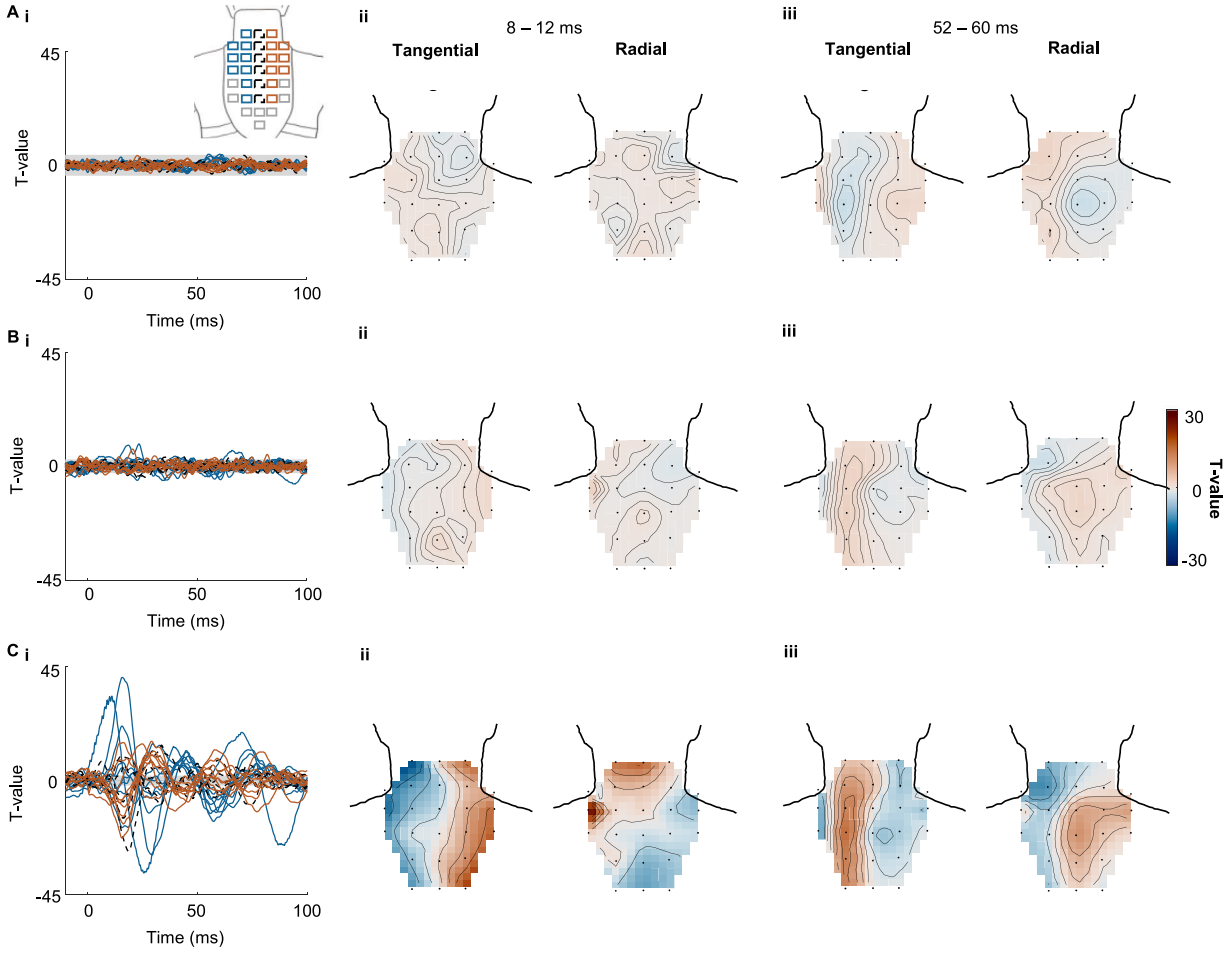

Fig. 3. Spinal cord evoked fields (SCEFs) in response to left wrist MNS over different stimulation conditions for participant A. **A.** 1 x, **B.** 1.5 x and **C.** 2.5 x motor threshold (MT). For each condition T-values for SCEFs from −10 to +100 around stimulation for radially orientated left (blue) and right (red) channels and tangentially orientated midline channels (black dotted) (i). The grey area (+/-4.06, 2.61 and 1.84 ms for Ai, Bi and Ci, respectively) represents where the signal is below the false discovery critical height threshold. The figure inlay in the top right of Ai illustrates the sensor map for all time courses. Magnetic field maps for T-values of SCEFs tangentially and radially orientated channels averaged over 8 – 12 ms (ii) and 52 – 60 ms (iii) post stimulation are illustrated. Average of 1695 trials for each condition. For display purposes, we show the SCEF time courses for tangentially orientated channels on the midline and the radially orientated channels to the left and right of this (illustrated by the sensor map in A), where the largest responses would be expected to occur based on a single current dipole within, and orientated along the axis of, the cervical spinal cord.

For the latter, OP-MSG field changes illustrated in Fig. 1D show how although the response peaks at 17 ms, it begins earlier, with an initial deflection at 11 ms that appears to blend into the larger response. For participant B, peak latency in the SCEF occurred at 11 ms post right wrist MNS.

3.3. Spinal cord evoked fields scale with intensity

To better understand the impact of stimulation intensity on the SCEF we used varying stimulator outputs for left wrist MNS in participant A. The latency of the peak components of the SCEF were extracted using the peak activity of the absolute maximum T-values across all spinal channels (both radial and tangential) that surpassed the FDR threshold.

Previous reports of SCEF use supramaximal MNS at the wrist and elbow to induce spinal responses (Akaza et al., 2021; Sumiya et al., 2017). Here, we found that 1.5 and 2.5 x motor threshold (MT) evoked SCEFs that increased with amplitude, respectively (Fig. 3B and C). Early responses peaked at 19 ms, for 1.5 x MT and 11 and 16 ms, for 2.5 x MT.

3.4. Late MNS spinal cord evoked fields show consistent latencies

In sessions with high suprathreshold MNS, where early SCEF were present, we also observed late SCEFs (>20 ms post stimulation) in both participants, illustrated in Fig. 4. Fig. 4Aii shows the maximum absolute T-values for participants A and B. A consistent series of peaks occurred at around 10, 18, 33 and 45 ms in both subjects. The observed field maps at these latencies are however more variable (see discussion). The long-latency trapezius muscle reflex response (supplementary figures 2 and 3) may have contributed to the variability at later latencies, but only partially overlapped with the MSEG responses.

In participant A, a strong late spinal response ~58 ms occurred in all sessions (both with and without early SCEFs following suprathreshold stimulation). Fig. 4F demonstrates the magnetic field distribution for the T-values of the ~58 ms SCEF, averaged over 52 – 60 ms post right wrist MNS. Field patterns are shown for tangentially orientated channels (peaking above spine) and radially orientated channels (peaking either side of spine with opposite polarity). The consistency of this component over sessions can be seen in Supplementary Figure 1.

Surrounding the central ~58 ms peak, in participant A, are two components with opposite polarity creating a triphasic waveform. The latency of the three peaks of the triphasic waveform, determined by the absolute maximum T-values were 43, 45, 45, 48 ms for peak 1; 56, 58, 58, 58 ms for peak 2; 71, 72, 70, 76 ms for peak 3 for right wrist MNS sessions 1 – 3 and 5, respectively, and 45, 40, 44 ms for peak 1; 57, 58, 57 ms for peak 2; 76, 70, 70 ms for peak 3 for left wrist MNS in session 3 and session 4, at 1.5 and 2.5 x MT, respectively.

Later spinal evoked fields were also seen in the session for participant B. A late triphasic waveform was seen following right wrist MNS in participant B, with peak latencies at 48, 70 and 89 ms post stimulation (Fig. 4E, F and G, lower panel).

3.5. Left and right MNS yields clear lateralized spinal cord evoked field

To determine if the SCEF observed was dependent on stimulus laterality, we recorded MNS at both the left and then right wrist in participant A during session 3, with 1130 trials each. T-values for the averaged SCEF for these two conditions can be seen in Fig. 5A. We found that the late ~58 ms response to left and right MNS exhibited lateralized SCEFs (Fig. 5A and B), with the largest response recorded on the side of the stimulation. This is emphasized by the field maps (Fig. 5B) for the radially orientated channels, which highlight how the dipolar pattern differs for left vs right MNS.

3.6. Source space analysis of left and right MNS

To further investigate late SCEF as well as the influence of stimulation side, we conducted a source analysis. We chose to explain the data with an equivalent current dipole (ECD), the simplest possible model. We fit this model to averaged SCEF from right wrist MNS in sessions 1 – 3 and 5 (labelled Right MNS 1, 2, 3 and 5) and the left wrist MNS in sessions 3 and two conditions in session 4 (labelled Left MNS 3, 4a and 4b), individually. There is clearly a great deal of work to be done on optimal forward and generative models of spinal cord function, however, it was encouraging to see that the optimal dipole fitting for 52 – 60 ms was consistent across sessions and lateralized to side of stimulation (Fig. 5C).

4. Discussion

We describe a wearable OPM system for the concurrent imaging of electrophysiological signals from the spinal cord and the brain. This study is based on peripheral nerve stimulation but opens the possibility for non-invasive precise imaging across the entire CNS in humans during a range of paradigms, including natural movement.

Recent work using MSG has described very fast spinal responses occurring 5.5 ms following MNS at the elbow (Sumiya et al., 2017) and 9.7 ms following MNS at the wrist (Akaza et al., 2021). Here, we saw early components 11 ms after MNS at the wrist, in sessions with high suprathreshold stimulation in both participants. These are consistent with the ascending volley, N9, at Erb's point and the cervical N13 spinal sensory evoked potential, recorded with surface electrodes (Restuccia et al., 1994). At this stage, the earliest detectable field changes reported in previous MSG studies likely stem from the conductivity changes as the depolarization propagates along the spinal nerve, through the intervertebral foramen, to the spinal cord (Akaza et al., 2021). Subsequent current may reflect the summed synaptic activity and currents from the dorsal column, followed by propagation of the signal along the spinal canal (Akaza et al., 2021; Iragui, 1984; Jones, 1977).

Although we found evidence for early spinal responses, they were not consistently recorded in all sessions, likely due to both external and physiological noise reducing the signal-to-noise ratio. Our ability to detect early spinal components may have been restricted by the limited bandwidth of our OPM system (Marquetand et al., 2021). The bandwidth of our system (up to 3 dB point) is 135 Hz and is due to the inherent trade-off between bandwidth and sensitivity in zero field OPMs (Dupont-Roc et al., 1969; Cohen-Tannoudji et al., 1970; Tierney et al., 2019). This does not preclude measurement of very fast changes (as the magnitude attenuation due to an effective first order filter is offset by the sensitivity gains from optimal sensor positioning). However, fast components in rapid succession (such as the stimulus artefact and early SCEF) may bleed into each other, making individual responses difficult to discern. A further limitation is the spatial coverage of our OPM sensors. As the number of sensors increases, the better spatial coverage will enable more precise identification of the different signal components of evoked activity.

In addition to these early responses, we also observed strong subsequent field changes attributed to the spinal cord. These later signal deflections are compatible with multi-channel evoked potentials and early work using an individual SQUID sensor positioned over the spinal cord (Mizutani and Kuriki, 1986; Nierula et al., 2022) and likely reflect a combination of intra-spinal mechanisms, descending feedback signals, and long-latency reflex activity, all from a mixture of anti- and orthodromic stimulation effects of the suprathreshold MNS used here. Long-latency reflexes (LLR) onset at ~50 ms in thenar EMG and can be elicited by both muscle and cutaneous afferent stimulation (Deuschl and Lücking, 1990). The first peak of the later triphasic spinal component we see here, occurred at ~40 ms after stimulation, which therefore, may contribute to the LLR. Conversely, these later responses could be reflective of the input of slower A-delta fibre activation (carrier of noxious information), which travel at 7 – 24 m/s (Tran et al., 2001; Obi et al., 2007), reaching the spinal cord. However, the participants did not report the stimulus being painful. Future work will address the specific contributions of these mechanisms to the signals, for which concurrent brain and spine imaging will be hugely beneficial.

The electrophysiological responses we report here, at both spinal and cortical levels, have previously been reported and are well-established as markers for clinical assessment (Prestor et al., 1991; Curt and Dietz, 1996; Cruse et al., 2014; Imajo et al., 2021). We primarily used

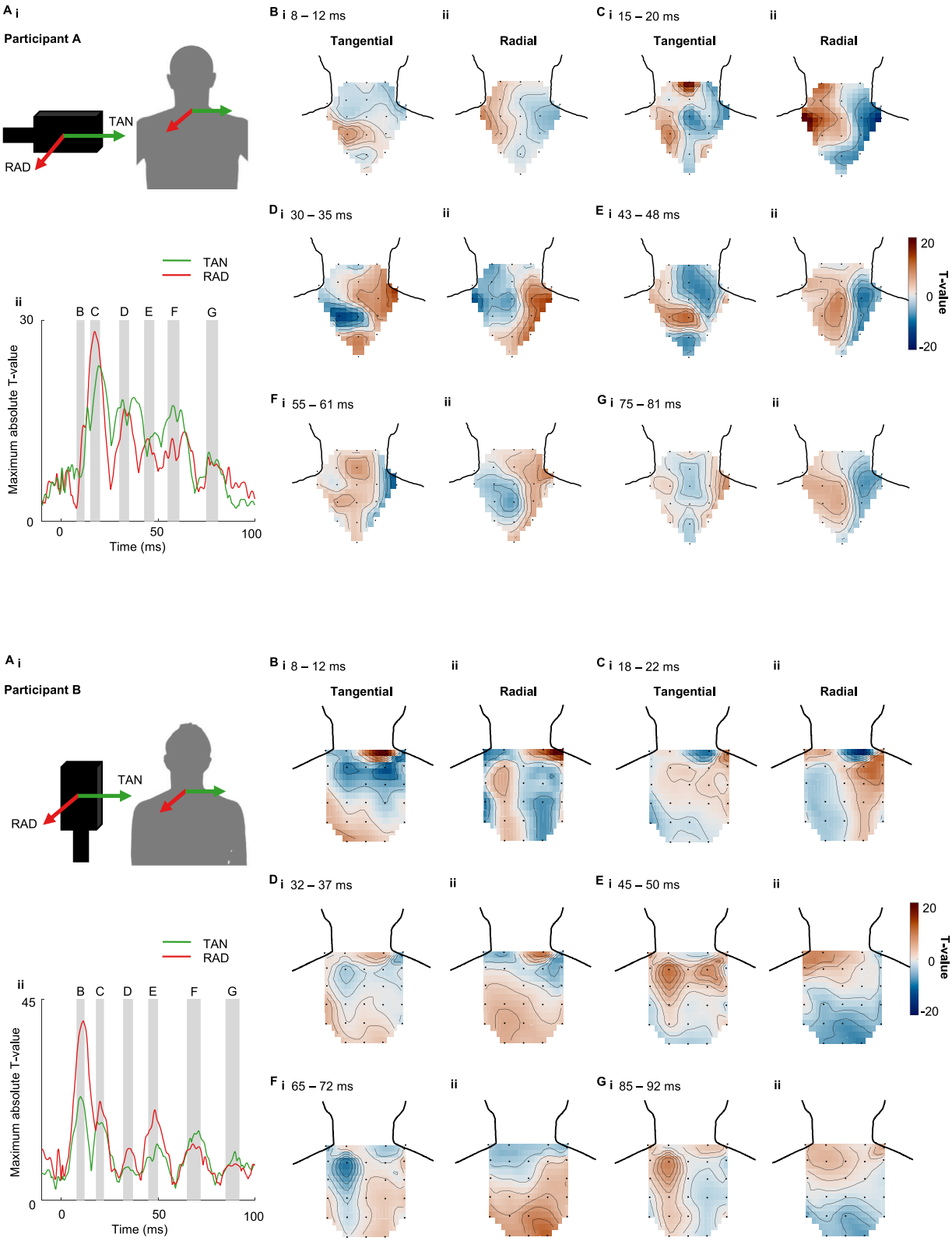

Fig. 4. Spinal cord evoked fields (SCEFs) following right wrist median nerve stimulation (MNS) in participants A (top) and B (lower). Ai. Optically pumped magnetometer (OPM) orientation during recording of SCEFs. ii. Maximum absolute T-values computed for radial and tangential OPM channels from −10 to +100 ms around right wrist MNS. Grey vertical bars highlight time windows that were identified to create the field maps in B – G. The dotted vertical line is at time of MNS. B. Magnetic field maps of T-values of the tangential (i) and radial (ii) OPM channels. Field maps in panels B, C, D, E, F and G correspond to the different time windows, as indicated. Note that for participant B three axes were recorded per sensor, however, only two are shown here for direct comparison with participant A.

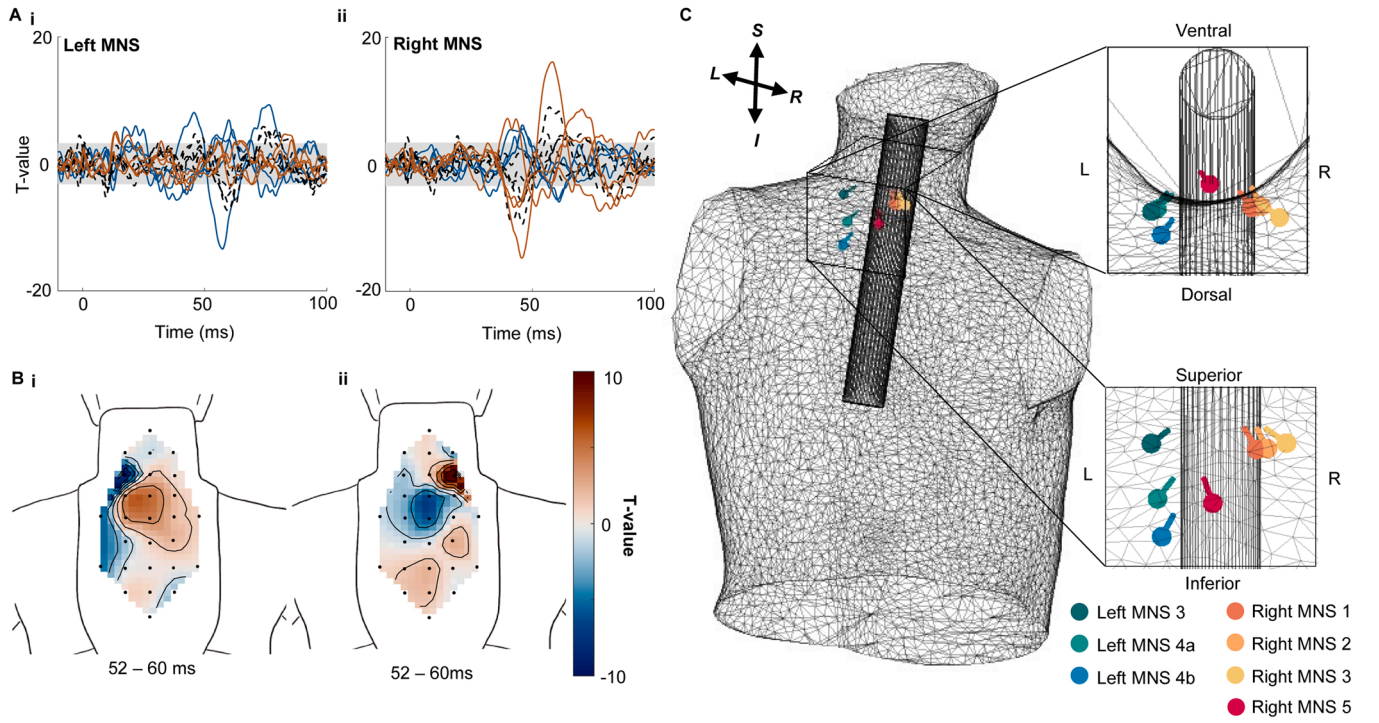

Fig. 5. Sensor and source level spinal cord evoked fields (SCEFs) to left and right median nerve stimulation (MNS). **A.** T-values for time courses of evoked fields for left (i) and right (ii) MNS during session 3 (each averaged over 1130 trials). Colours indicate channels located to the left (blue, radially orientated), to the right (red, radially orientated), or over the midline (black dotted, tangentially orientated), respectively. The grey area represents where the signal is below the false discovery critical height threshold. **B.** Magnetic field maps of T-values for radially oriented channels averaged over 52 – 60 ms post stimulation for left (i) and right (ii) MNS at the wrist. **C.** Optimal dipole fit for the 52 – 60 ms SCEF component, identified using equivalent current dipole (ECD) fitting for four right MNS sessions (Right MNS 1, 2, 3 and 5; 2260, 2260, 1130 and 2260 trials, respectively) and three left MNS sessions (Left MNS 3, 4a and 4b; 1130, 1695 and 1695 trials, respectively), displayed within the body model relative to a cylinder used to approximate spinal cord location.

peripheral nerve stimulation to establish a proof of principle for the ability of OPMs to detect spinal activity in humans, and to demonstrate the ability for concurrent electrophysiological assessment across the entire CNS. While here initially conducted in a small number of subjects only, we believe this now opens the exciting opportunity to study the spinal responses in a wide range of paradigms in larger cohorts and patient groups.

There are several limitations and challenges we want to point out. Although the time-series observed between subjects were similar, the spatial profiles of these responses were unexpectedly inconsistent. There are several possible reasons for this inconsistency. It may be that the cervical spinal cord, with multiple conductivity boundaries due to bone, cerebrospinal fluid and the thoracic cavity gives rise to magnetic field profiles which are highly subject specific, with muscle and cardiorespiratory artefacts contributing to signal noise. During background levels of muscle contraction (~20% maximum voluntary contraction), long-latency reflexes can be elicited in the trapezius muscle at similar latencies to the late spinal responses we capture here (Alexander and Harrison, 2003; Tataroglu et al., 2011). In our case, the temporal profiles of these reflex responses did not match the responses seen with our MSEG recordings (see Supplementary Figures 2 and 3), but their partial overlap may still contribute to some of the late responses seen with MSEG. Future work using source reconstruction or other spatial filtering techniques may help address the specific contributions from different sources.

Based on the recent high-density electrophysiological study (Nierula et al., 2022) it appears that the dominant electrical components are radial to the surface of the back. Small inter-individual deviations in the orientation of these radial components may also have large effects on the measured field. This also impacts on the type of theoretical source model. Here we used simple volume conductor and source models which clearly warrant elaboration. In this work, we have approximated current flow as dipolar. We know from the complex organization of neurons within the cord that this is unlikely to be the case (given perfect resolution and sensitivity). The dipole model is therefore the simplest approximation showing the net direction of current flow at an instant in time. We hope that improvement in our recording and source modelling (including registration to the anatomy) will allow us to posit more complex source models in future.

Going forward, solutions based on boundary/finite element models that will best account for the spinal anatomy are likely to improve source estimation. Future work could also be devoted to new beamformer schemes, e.g., the recursive null-steering beamformer (Kumihashi and Sekihara, 2010) implemented in Sumiya et al. (2017) and Akaza et al. (2021), to attenuate stimulation artefacts or indeed simply different experimental paradigms. Despite the current limitations, however, we were able to show lateralized responses to peripheral nerve stimulation, with dipole locations that were compatible with the known anatomy of the spinal cord, and with latencies matching previous reports using surface electrodes or MSG (Akaza et al., 2021; Mizutani and Kuriki, 1986).

Further, technical aspects in OPM data acquisition will continue to improve and yield higher SNR. For example, we expect that with a larger number of sensors, continuing the use of triaxial rather than dual-axis devices (Brookes et al., 2021; Tierney et al., 2022), we will be able to better characterize both the signal and environmental noise space. Also, although OPM sensitivity does begin to decline at 130 Hz, it does so only as a first order filter (i.e., a halving of amplitude for every doubling of frequency). Additionally, optimizing the orientation and location of the OPM sensors will help to distinguish varying aspects of the spinal response, such as activity in the dorsal root ganglia, intraspinal processing and the ascending wave. Increasing the number of sensors used

to provide wider coverage, along with the ongoing reduction in OPM size, will enable high density recordings at a reduced weight, improving the feasibility and tolerability for unconstrained assessment of brain and spinal physiology, and finally, future recordings may also aim to measure breathing and heart rates and back-muscle activity to aid in noise reduction techniques.

In the present study we chose to use peripheral stimulation to probe the sensorimotor system, which benefits from the time-locked nature of the response. Future progressions of this research should study the cortico-spinal interactions of movement generation, but this is not without challenges. Due to the multiple stages in motor processing prior to the spinal cord, activity may be more temporally dispersed, potentially leading to weaker signals. Additionally, movement artefacts will create challenges in data processing, however, previous OP-MEG work has identified analysis pipelines to overcome this (Seymour et al., 2021, 2022). Moreover, changes in the frequency domain of the signal may provide greater insight into motor processing at the spinal level, which along with OP-MEG recordings could illuminate cortico-spinal interactions (Oya et al., 2020).

The work here builds on the knowledge of the classical SEP through measurement of its magnetic analogue. The magnetic signal, although difficult to measure, has the advantage that it is minimally distorted by surrounding tissue. The clinical potential of this technique has been clearly demonstrated using super-conducting sensors (Akaza et al., 2021; Miyano et al., 2020; Sumiya et al., 2017). Here we expand this work to OPMs; the main advantage of which is their flexibility (simultaneous measurements of brain and cord) and wearability (potentially wearable and of use whilst subject is behaving naturally).

One major advance of MSEG over existing approaches to spinal electrophysiological recordings is that these sensors can be worn, offering widespread usability to study the electrophysiology of the spinal cord not only in healthy adults but a range of cohorts such as children or many disorders accompanied by pathological movement (Hill et al., 2019; Vivekananda et al., 2020). The potential for studying movement is particularly beneficial in patient groups that cannot easily remain still or movement is impaired. One of the most transformative aspects of OPM recordings is that high quality recordings can be obtained in a wide range of postures, and even during relatively large and unpredictable movements (Holmes et al., 2018; Boto et al., 2018; Hill et al., 2019; Roberts et al., 2019; Seymour et al., 2021). Therefore, this technology lends itself to the study of motor development as well as pathology in conditions such as stroke, Parkinson's disease and neurogenerative disorders. The flexibility of OPM sensor arrangement also means that sensor arrays are not limited to the cervical spinal cord, as done here, but can easily be configured for thoracic and lumbosacral spinal imaging, or indeed to image the entire spinal cord, whilst additionally allowing for recording brain activity with high precision.

A wide range of disorders and pathologies affect the spinal cord and cortico-spinal interplay, including spinal cord injury (SCI), stroke, traumatic brain injury, or the spinal grey matter degeneration seen in amyotrophic lateral sclerosis (Nagamoto-Combs et al., 2010; Cohen-Adad et al., 2013; Grabher et al., 2015; Chen et al., 2018). Basic understanding of the underlying mechanisms of the impairments caused by these pathologies, the response to treatment, and basis of recovery will benefit from imaging the entire CNS. The ability for high-precision electrophysiology of the entire CNS will transform our understanding of the human spinal cord.

Funding

This work was initiated (and T.M.T. funded) through a Wellcome Collaborative Award (203257/Z/16/Z, 203257/B/16/Z) and is now funded through a Wellcome Technology Development award (223736/Z/21/Z). G.C.O. was funded through EPSRC (EP/T001046/1) funding from the Quantum Technology hub in sensing and timing (sub-award QTPRF02). L.C.M. was funded through Medical Research Council (MR/N013867/1). C.Z. was funded through Brain Research UK (201718-13). The Wellcome Centre for Human Neuroimaging is supported by core funding from the Wellcome Trust (203147/Z/16/Z).

CRediT authorship contribution statement

Lydia Catherine Mardell: Conceptualization, Formal analysis, Investigation, Methodology, Project administration, Software, Visualization, Writing – original draft, Writing – review & editing. **Meaghan Elizabeth Spedden:** Conceptualization, Formal analysis, Investigation, Methodology, Software, Writing – review & editing. **George O′Neill:** Conceptualization, Formal analysis, Investigation, Methodology, Software, Writing – review & editing. **Tim Tierney:** Conceptualization, Formal analysis, Investigation, Methodology, Writing – review & editing. **Ryan Timms:** Investigation, Writing – review & editing. **Catharina Zich:** Writing – review & editing. **Gareth Barnes:** Funding acquisition, Methodology, Project administration, Software, Supervision, Writing – original draft, Writing – review & editing, Conceptualization, Formal analysis. **Sven Bestmann:** Writing – review & editing, Writing – original draft, Supervision, Conceptualization, Funding acquisition, Methodology.

Declaration of Competing Interest

The authors declare no competing interests.

Data Availability

Data will be made available on request.

Acknowledgments

We would like to acknowledge the support of Mark Lim of Chalk Studios in designing the 3D printed scanner-casts used in this study and thank Blake Hale for conducting the clinical SEP recordings. We would also like to thank Dr Adachi and Professor Kawabata from the Kanazawa Institute of Technology and Tokyo Medical and Dental University in Japan for their support and advice in the conception of this project.

Appendix A. Supporting information

Supplementary data associated with this article can be found in the online version at doi:10.1016/j.jneumeth.2024.110131.

References

Adachi, Y., Oyama, D., Kawabata, S., Sekihara, K., Haruta, Y., Uehara, G., 2013. Magnetospinography: instruments and application to functional imaging of spinal cords. *IEICE Trans. Electron.* E96. C. 326–333.

Akaza, M., Kawabata, S., Ozaki, I., Miyano, Y., Watanabe, T., Adachi, Y., Sekihara, K., Sumi, Y., Yokota, T., 2021. Noninvasive measurement of sensory action currents in the cervical cord by magnetospinography. Clin. Neurophysiol. 132, 382–391. https://doi.org/10.1016/j.clinph.2020.11.029.

Alexander, C.M., Harrison, P.J., 2002. The bilateral reflex control of the trapezius muscle in humans. Exp. Brain Res. https://doi.org/10.1007/s00221-001-0951-2.

Alexander, C.M., Harrison, P.J., 2003. Reflex connections from forearm and hand afferents to shoulder girdle muscles in humans. Exp. Brain Res 148, 277–282.

Allison, T., Mccarthy, G., Wood, C.C., Jones, S.J., 1991. Potentials evoked in human and monkey cerebral cortex by stimulation of the median nerve: A review of scalp and intracranial recordings. Brain. https://doi.org/10.1093/brain/114.6.2465.

Altarev, I., Fierlinger, P., Lins, T., Marino, M.G., Nießen, B., Petzoldt, G., Reisner, M., Stuiber, S., Sturm, M., Taggart Singh, J., Taubenheim, B., Rohrer, H.K., Schläpfer, U., 2015. Minimizing magnetic fields for precision experiments. J. Appl. Phys. https://doi.org/10.1063/1.4922671.

Baliki, M.N., Baria, A.T., Vania Apkarian, A., 2011. The Cortical Rhythms of Chronic Back Pain. J. Neurosci. https://doi.org/10.1523/JNEUROSCI.1984-11.2011.

Barry, D.N., Tierney, T.M., Holmes, N., Boto, E., Roberts, G., Leggett, J., Bowtell, R., Brookes, M.J., Barnes, G.R., Maguire, E.A., 2019. Imaging the human hippocampus with optically-pumped magnetoencephalography. Neuroimage. https://doi.org/10.1016/j.neuroimage.2019.116192.

Boto, E., Bowtell, R., Krüger, P., Fromhold, T.M., Morris, P.G., Meyer, S.S., Barnes, G.R., Brookes, M.J., 2016. On the potential of a new generation of magnetometers for

MEG: a beamformer simulation study. PLoS One. https://doi.org/10.1371/journal.pone.0157655.
Boto, E., Shah, V., Hill, R.M., Rhodes, N., Osborne, J., Doyle, C., Holmes, N., Rea, M., Leggett, J., Bowtell, R., Brookes, M.J., 2022. Triaxial detection of the neuromagnetic field using optically-pumped magnetometry: feasibility and application in children. Neuroimage. https://doi.org/10.1016/j.neuroimage.2022.119027.
Boto, E., Meyer, S.S., Shah, V., Alem, O., Knappe, S., Kruger, P., Fromhold, T.M., Lim, M., Glover, P.M., Morris, P.G., Bowtell, R., Barnes, G.R., Brookes, M.J., 2017. A new generation of magnetoencephalography: Room temperature measurements using optically-pumped magnetometers. Neuroimage 149, 404–414.
Boto, E., Holmes, N., Leggett, J., Roberts, G., Shah, V., Meyer, S.S., Muñoz LD, Mullinger, K.J., Tierney, T.M., Bestmann, S., Barnes, G.R., Bowtell, R., Brookes, M.J., 2018. Moving magnetoencephalography towards real-world applications with a wearable system. Nature 555, 657–661.
Boto, E., Seedat, Z.A., Holmes, N., Leggett, J., Hill, R.M., Roberts, G., Shah, V., Fromhold, T.M., Mullinger, K.J., Tierney, T.M., Barnes, G.R., Bowtell, R., Brookes, M.J., 2019. Wearable neuroimaging: combining and contrasting magnetoencephalography and electroencephalography. Neuroimage. https://doi.org/10.1016/j.neuroimage.2019.116099.
Brookes, M.J., Leggett, J., Rea, M., Hill, R.M., Holmes, N., Boto, E., Bowtell, R., 2022. Magnetoencephalography with optically pumped magnetometers (OPM-MEG): the next generation of functional neuroimaging. Trends Neurosci. 45, 621–634.
Brookes, M.J., Boto, E., Rea, M., Shah, V., Osborne, J., Holmes, N., Hill, R.M., Leggett, J., Rhodes, N., Bowtell, R., 2021. Theoretical advantages of a triaxial optically pumped magnetometer magnetoencephalography system. Neuroimage. https://doi.org/10.1016/j.neuroimage.2021.118025.
Bu, Y., Prince, J., Mojtahed, H., Kimball, D., Shah, V., Coleman, T., Sarkar, M., Rao, R., Huang, M., Schwindt, P., Borna, A., Lerman, I., 2022. Peripheral Nerve Magnetoneurography With Optically Pumped Magnetometers. Front Physiol. https://doi.org/10.3389/fphys.2022.798376.
Chander, B.S., Deliano, M., Azañón, E., Büntjen, L., Stenner, M.P., 2022. Non-invasive recording of high-frequency signals from the human spinal cord. Neuroimage. https://doi.org/10.1016/j.neuroimage.2022.119050.
Chen, X., Xie, P., Zhang, Y., Chen, Y., Cheng, S., Zhang, L., 2018. Abnormal functional corticomuscular coupling after stroke. Neuroimage Clin. https://doi.org/10.1016/j.nicl.2018.04.004.
Claus, S., Velis, D., Lopes da Silva, F.H., Viergever, M.A., Kalitzin, S., 2012. High frequency spectral components after secobarbital: the contribution of muscular origin-a study with MEG/EEG. Epilepsy Res. https://doi.org/10.1016/j.eplepsyres.2012.02.002.
Cohen-Adad, J., Mendili, M.M. el, Morizot-Koutlidis, R., Lehéricy, S., Meininger, V., Blancho, S., Rossignol, S., Benali, H., Pradat, P.F., 2013. Involvement of spinal sensory pathway in ALS and specificity of cord atrophy to lower motor neuron degeneration. Amyotroph. Lateral Scler. Front. Degener. https://doi.org/10.3109/17482968.2012.701308.
Cohen-Tannoudji, C., Dupont-Roc, J., Haroche, S., Laloë, F., 1970. Diverses résonances de croisement de niveaux sur des atomes pompés optiquement en champ nul. I. Théorie. Rev. De. Phys. Appliquée. https://doi.org/10.1051/rphysap:019700050109500.
Cracco, R.Q., 1973. Spinal evoked response: Peripheral nerve stimulation in man. Electro Clin. Neurophysiol. https://doi.org/10.1016/0013-4694(73)90195-8.
Cruse, D., Norton, L., Gofton, T., Young, G.B., Owen, A.M., 2014. Positive prognostication from median-nerve somatosensory evoked cortical potentials. Neurocrit Care. https://doi.org/10.1007/s12028-014-9982-y.
Curt, A., Dietz, V., 1996. Traumatic cervical spinal cord injury: relation between somatosensory evoked potentials, neurological deficit, and hand function. Arch. Phys. Med Rehabil. https://doi.org/10.1016/S0003-9993(96)90219-1.
Dauleac, C., Frindel, C., Mertens, P., Jacquesson, T., Cotton, F., 2020. Overcoming challenges of the human spinal cord tractography for routine clinical use: a review. Neuroradiology. https://doi.org/10.1007/s00234-020-02442-8.
De Oliveira, H.M., Silsby, M., Jaiser, S.R., Lai, H.M., Pavey, N., Kiernan, M.C., Williams, T.L., Vucic, S., Baker, M.R., 2022. Electrodiagnostic findings in facial onset sensory motor neuronopathy (FOSMN). Clin. Neurophysiol. 140, 228–238.
Derosiere, G., Vassiliadis, P., Duque, J., 2020. Advanced TMS approaches to probe corticospinal excitability during action preparation. Neuroimage. https://doi.org/10.1016/j.neuroimage.2020.116746.
Desmedt, J.E., Nguyen Tran Huy, Bourguet, M., 1983. The cognitive P40, N60 and P100 components of somatosensory evoked potentials and the earliest electrical signs of sensory processing in man. Electro Clin. Neurophysiol. https://doi.org/10.1016/0013-4694(83)90252-3.
Deuschl, G., Lücking, C.H., 1990. Physiology and clinical applications of hand muscle reflexes. Electro Clin. Neurophysiol. Suppl. https://doi.org/10.1016/b978-0-444-81352-7.50012-1.
Dupont-Roc, J., Haroche, S., Cohen-Tannoudji, C., 1969. Detection of very weak magnetic fields (10-9gauss) by 87Rb zero-field level crossing resonances. Phys. Lett. A. https://doi.org/10.1016/0375-9601(69)90480-0.
Fife, A.A., et al., 1999. Synthetic gradiometer systems for MEG. IEEE Trans. Appl. Supercond. https://doi.org/10.1109/77.783919.
Filli, L., Schwab, M.E., 2012. The rocky road to translation in spinal cord repair. Ann. Neurol. https://doi.org/10.1002/ana.23630.
Freund, P., Schneider, T., Nagy, Z., Hutton, C., Weiskopf, N., Friston, K., Wheeler-Kingshott, C.A., Thompson, A.J., 2012. Degeneration of the injured cervical cord is associated with remote changes in corticospinal tract integrity and upper limb impairment. PLoS One. https://doi.org/10.1371/journal.pone.0051729.
Fujimoto, H., Kaneko, K., Taguchi, T., Ofuji, A., Yonemura, H., Kawai, S., 2001. Differential recording of upper and lower cervical N13 responses and their contribution to scalp recorded responses in median nerve somatosensory evoked potentials. J. Neurol. Sci. https://doi.org/10.1016/S0022-510X(01)00509-3.
Furby, J., Hayton, T., Anderson, V., Altmann, D., Brenner, R., Chataway, J., Hughes, R.A. C., Smith, K.J., Miller, D.H., Kapoor, R., 2008. Magnetic resonance imaging measures of brain and spinal cord atrophy correlate with clinical impairment in secondary progressive multiple sclerosis. Mult. Scler. https://doi.org/10.1177/1352458508093617.
García-Larrea, L., Bastuji, H., Mauguière, F., 1991. Mapping study of somatosensory evoked potentials during selective spatial attention. Electroencephalogr. Clin. Neurophysiol. / Evoked Potentials. https://doi.org/10.1016/0168-5597(91)90122-E.
Giove, F., Garreffa, G., Giulietti, G., Mangia, S., Colonnese, C., Maraviglia, B., 2004. Issues about the fMRI of the human spinal cord. *Magn. Reson. Imaging*.
Grabher, P., Callaghan, M.F., Ashburner, J., Weiskopf, N., Thompson, A.J., Curt, A., Freund, P., 2015. Tracking sensory system atrophy and outcome prediction in spinal cord injury. Ann. Neurol. https://doi.org/10.1002/ana.24508.
Hill, R.M., Boto, E., Holmes, N., Hartley, C., Seedat, Z.A., Leggett, J., Roberts, G., Shah, V., Tierney, T.M., Woolrich, M.W., Stagg, C.J., Barnes, G.R., Bowtell, R.R., Slater, R., Brookes, M.J., 2019. A tool for functional brain imaging with lifespan compliance. Nat. Commun. https://doi.org/10.1038/s41467-019-12486-x.
Holmes, N., Leggett, J., Boto, E., Roberts, G., Hill, R.M., Tierney, T.M., Shah, V., Barnes, G.R., Brookes, M.J., Bowtell, R., 2018. A bi-planar coil system for nulling background magnetic fields in scalp mounted magnetoencephalography. Neuroimage. https://doi.org/10.1016/j.neuroimage.2018.07.028.
Ibáñez, J., Del Vecchio, A., Rothwell, J.C., Baker, S.N., Farina, D., 2021. Only the fastest corticospinal fibers contribute to B corticomuscular coherence. J. Neurosci. https://doi.org/10.1523/JNEUROSCI.2908-20.2021.
Iivanainen, J., Stenroos, M., Parkkonen, L., 2017. Measuring MEG closer to the brain: Performance of on-scalp sensor arrays. Neuroimage. https://doi.org/10.1016/j.neuroimage.2016.12.048.
Imajo, Y., Kanchiku, T., Suzuki, H., Nishida, N., Funaba, M., Taguchi, T., Sakai, T., 2021. Assessment of spinal cord relative vulnerability in C4–C5 compressive cervical myelopathy using multi-modal spinal cord evoked potentials and neurological findings. J. Spinal Cord. Med 44, 541–548.
Iragui, V.J., 1984. The cervical somatosensory evoked potential in man: Far-field, conducted and segmental components. Electro Clin. Neurophysiol. https://doi.org/10.1016/0013-4694(84)90124-X.
Jones, S.J., 1977. Short latency potentials recorded from the neck and scalp following median nerve stimulation in man. Electro Clin. Neurophysiol. 43, 853–863.
Kakigi, R., 1994. Somatosensory evoked magnetic fields following median nerve stimulation. Neurosci. Res. https://doi.org/10.1016/0168-0102(94)90034-5.
Karbasforoushan, H., Cohen-Adad, J., Dewald, J.P.A., 2019. Brainstem and spinal cord MRI identifies altered sensorimotor pathways post-stroke. Nat. Commun. 10, 3524.
Kawabata, S., Komori, H., Mochida, K., Harunobu, O., Shinomiya, K., 2002. Visualization of conductive spinal cord activity using a biomagnetometer. Spine (Philos. Pa 1976). https://doi.org/10.1097/00007632-200203010-00007.
Keil, J., Timm, J., SanMiguel, I., Schulz, H., Obleser, J., Schönwiesner, M., 2014. Cortical brain states and corticospinal synchronization influence TMS-evoked motor potentials. J. Neurophysiol. https://doi.org/10.1152/jn.00387.2013.
Kinany, N., Pirondini, E., Micera, S., van de Ville, D., 2022. Spinal Cord fMRI: A New Window into the Central Nervous System. Neuroscientist. https://doi.org/10.1177/10738584221101827.
Kumihashi, I., Sekihara, K., 2010. Array-gain constraint minimum-norm spatial filter with recursively updated gram matrix for biomagnetic source imaging. IEEE Trans. Biomed. Eng. https://doi.org/10.1109/TBME.2010.2040735.
Lamy, J.C., Wargon, I., Mazevet, D., Ghanim, Z., Pradat-Diehl, P., Katz, R., 2009. Impaired efficacy of spinal presynaptic mechanisms in spastic stroke patients. Brain. https://doi.org/10.1093/brain/awn310.
Landelle, C., Dahlberg, L.S., Lungu, O., Misic, B., De Leener, B., Doyon, J., 2023. Altered spinal cord functional connectivity associated with Parkinson's disease progression. Mov. Disord. https://doi.org/10.1002/mds.29354.
Lin, C.H., Tierney, T.M., Holmes, N., Boto, E., Leggett, J., Bestmann, S., Bowtell, R., Brookes, M.J., Barnes, G.R., Miall, R.C., 2019. Using optically pumped magnetometers to measure magnetoencephalographic signals in the human cerebellum. J. Physiol. https://doi.org/10.1113/JP277899.
Marquetand, J., Middelmann, T., Dax, J., Baek, S., Sometti, D., Grimm, A., Lerche, H., Martin, P., Kronlage, C., Siegel, M., Braun, C., Broser, P., 2021. Optically pumped magnetometers reveal fasciculations non-invasively. Clin. Neurophysiol. https://doi.org/10.1016/j.clinph.2021.06.009.
Miyano, Y., Kawabata, S., Akaza, M., Sekihara, K., Hoshino, Y., Sasaki, T., Watanabe, T., Kim, S., Sato, S., Mitani, Y., Adachi, Y., Okawa, A., 2020. Visualization of electrical activity in the cervical spinal cord and nerve roots after ulnar nerve stimulation using magnetospinography. Clin. Neurophysiol. 131, 2460–2468. https://doi.org/10.1016/j.clinph.2020.07.009.
Mizutani, Y., Kuriki, S., 1986. Somatically evoked magnetic fields in the vicinity of the neck. IEEE Trans. Biomed. Eng. https://doi.org/10.1109/TBME.1986.325738.
Moore, K.A., Kohno, T., Karchewski, L.A., Scholz, J., Baba, H., Woolf, C.J., 2002. Partial peripheral nerve injury promotes a selective loss of GABAergic inhibition in the superficial dorsal horn of the spinal cord. J. Neurosci. https://doi.org/10.1523/jneurosci.22-15-06724.2002.
Muthukumaraswamy, S.D., 2013. High-frequency brain activity and muscle artifacts in MEG/EEG: A review and recommendations. Front Hum. Neurosci. https://doi.org/10.3389/fnhum.2013.00138.
Nagamoto-Combs, K., Morecraft, R.J., Darling, W.G., Combs, C.K., 2010. Long-term gliosis and molecular changes in the cervical spinal cord of the rhesus monkey after traumatic brain injury. J. Neurotrauma. https://doi.org/10.1089/neu.2009.0966.

Nierula, B., Stephani, T., Kaptan, M., Mouraux, A., Maess, B., Curio, G., Nikulin, V.V., Eippert, F., 2022. Non-invasive multi-channel electrophysiology of the human spinal cord-assessing somatosensory processing from periphery to cortex. bioRxiv. https://doi.org/10.1101/2022.12.05.519148.

Nolte, G., 2003. The magnetic lead field theorem in the quasi-static approximation and its use for magnetoenchephalography forward calculation in realistic volume conductors. Phys. Med Biol. https://doi.org/10.1088/0031-9155/48/22/002.

Obi, T., Takatsu, M., Yamazaki, K., Kuroda, R., Terada, T., Mizoguchi, K., 2007. Conduction velocities of Aδ-fibers and C-fibers in human peripheral nerves and spinal cord after CO2 laser stimulation. J. Clin. Neurophysiol. https://doi.org/10.1097/WNP.0b013e318038f45f.

Oostenveld, R., Fries, P., Maris, E., Schoffelen, J.M., 2011. FieldTrip: Open source software for advanced analysis of MEG, EEG, and invasive electrophysiological data. Comput. Intell. Neurosci. https://doi.org/10.1155/2011/156869.

Osborne J., Orton J., Alem O. & Shah V. (2018). Fully integrated, standalone zero field optically pumped magnetometer for biomagnetism.

Oya, T., Takei, T., Seki, K., 2020. Distinct sensorimotor feedback loops for dynamic and static control of primate precision grip. Commun. Biol. https://doi.org/10.1038/s42003-020-0861-0.

Panara, V., Navarra, R., Mattei, P.A., Piccirilli, E., Bartoletti, V., Uncini, A., Caulo, M., 2019. Correlations between cervical spinal cord magnetic resonance diffusion tensor and diffusion kurtosis imaging metrics and motor performance in patients with chronic ischemic brain lesions of the corticospinal tract. Neuroradiology. https://doi.org/10.1007/s00234-018-2139-5.

Prestor, B., Žgur, T., Dolenc, V. v, 1991. Subpially recorded cervical spinal cord evoked potentials in syringomyelia. Electroencephalogr. Clin. Neurophysiol. / Evoked Potentials. https://doi.org/10.1016/0168-5597(91)90153-O.

Restuccia, D., Valeriani, M., di Lazzaro, V., Tonali, P., Mauguiere, F., 1994. Somatosensory evoked potentials after multisegmental upper limb stimulation in diagnosis of cervical spondylotic myelopathy. J. Neurol. Neurosurg. Psychiatry 57, 301–308.

Roberts, G., Holmes, N., Alexander, N., Boto, E., Leggett, J., Hill, R.M., Shah, V., Rea, M., Vaughan, R., Maguire, E.A., Kessler, K., Beebe, S., Fromhold, M., Barnes, G.R., Bowtell, R., Brookes, M.J., 2019. Towards OPM-MEG in a virtual reality environment. Neuroimage. https://doi.org/10.1016/j.neuroimage.2019.06.010.

Sakaki, K., Hoshino, Y., Kawabata, S., Adachi, Y., Watanabe, T., Sekihara, K., Ishii, S., Tomori, M., Tomizawa, S., Enomoto, M., Okawa, A., 2020. Evaluation of neural activity by magnetospinography with 3D sensors. Clin. Neurophysiol. https://doi.org/10.1016/j.clinph.2020.02.025.

Seymour, R.A., Alexander, N., Mellor, S., O'Neill, G.C., Tierney, T.M., Barnes, G.R., Maguire, E.A., 2021. Using OPMs to measure neural activity in standing, mobile participants. Neuroimage. https://doi.org/10.1016/j.neuroimage.2021.118604.

Seymour, R.A., Alexander, N., Mellor, S., O'Neill, G.C., Tierney, T.M., Barnes, G.R., Maguire, E.A., 2022. Interference suppression techniques for OPM-based MEG: opportunities and challenges. Neuroimage 247, 118834.

Sprenger, C., Finsterbusch, J., Büchel, C., 2015. Spinal cord-midbrain functional connectivity is related to perceived pain intensity: a combined spino-cortical fMRI study. J. Neurosci. https://doi.org/10.1523/JNEUROSCI.4897-14.2015.

Stroman, P.W., et al., 2014. The current state-of-the-art of spinal cord imaging: Methods. Neuroimage. https://doi.org/10.1016/j.neuroimage.2013.04.124.

Sumiya, S., Kawabata, S., Hoshino, Y., Adachi, Y., Sekihara, K., Tomizawa, S., Tomori, M., Ishii, S., Sakaki, K., Ukegawa, D., Ushio, S., Watanabe, T., Okawa, A., 2017. Magnetospinography visualizes electrophysiological activity in the cervical spinal cord. Sci. Rep. 7, 2192. https://doi.org/10.1038/s41598-017-02406-8.

Tataroglu, C., Kuçuk, F.K., Ozkul, A., 2011. Upper and lower extremity proprioceptive inputs modulate EMG activity of the trapezius. J. Electromyogr. Kinesiol. https://doi.org/10.1016/j.jelekin.2010.09.011.

Tierney, T.M., Mellor, S., O'Neill, G.C., Timms, R.C., Barnes, G.R., 2022. Spherical harmonic based noise rejection and neuronal sampling with multi-axis OPMs. Neuroimage. https://doi.org/10.1016/j.neuroimage.2022.119338.

Tierney, T.M., Alexander, N., Mellor, S., Holmes, N., Seymour, R., O'Neill, G.C., Maguire, E.A., Barnes, G.R., 2021a. Modelling optically pumped magnetometer interference in MEG as a spatially homogeneous magnetic field. Neuroimage. https://doi.org/10.1016/j.neuroimage.2021.118484.

Tierney, T.M., Holmes, N., Mellor, S., López, J.D., Roberts, G., Hill, R.M., Boto, E., Leggett, J., Shah, V., Brookes, M.J., Bowtell, R., Barnes, G.R., 2019. Optically pumped magnetometers: from quantum origins to multi-channel magnetoencephalography. Neuroimage. https://doi.org/10.1016/j.neuroimage.2019.05.063.

Tierney, T.M., Levy, A., Barry, D.N., Meyer, S.S., Shigihara, Y., Everatt, M., Mellor, S., Lopez, J.D., Bestmann, S., Holmes, N., Roberts, G., Hill, R.M., Boto, E., Leggett, J., Shah, V., Brookes, M.J., Bowtell, R., Maguire, E.A., Barnes, G.R., 2021b. Mouth magnetoencephalography: a unique perspective on the human hippocampus. Neuroimage 225, 117443.

Tran, T.D., Lam, K., Hoshiyama, M., Kakigi, R., 2001. A new method for measuring the conduction velocities of Aβ-, Aδ- and C-fibers following electric and CO2 laser stimulation in humans. Neurosci. Lett. https://doi.org/10.1016/S0304-3940(01)01639-1.

Urasaki, E., Wada, S.-I., Kadoya, C., Tokimura, T., Yokota, A., Matsuoka, S., Fukumura, A., Hamada, S., 1990. Skin and epidural recording of spinal somatosensory evoked potentials following median nerve stimulation: correlation between the absence of spinal N13 and impaired pain sense. J. Neurol. 237, 410–415.

Ushio, S., Hoshino, Y., Kawabata, S., Adachi, Y., Sekihara, K., Sumiya, S., Ukegawa, D., Sakaki, K., Watanabe, T., Hasegawa, Y., Okawa, A., 2019. Visualization of the electrical activity of the cauda equina using a magnetospinography system in healthy subjects. Clin. Neurophysiol. https://doi.org/10.1016/j.clinph.2018.11.001.

Vahdat, S., Khatibi, A., Lungu, O., Finsterbusch, J., Büchel, C., Cohen-Adad, J., Marchand-Pauvert, V., Doyon, J., 2020. Resting-state brain and spinal cord networks in humans are functionally integrated. PLoS Biol. https://doi.org/10.1371/journal.pbio.3000789.

Vivekananda, U., Mellor, S., Tierney, T.M., Holmes, N., Boto, E., Leggett, J., Roberts, G., Hill, R.M., Litvak, V., Brookes, M.J., Bowtell, R., Barnes, G.R., Walker, M.C., 2020. Optically pumped magnetoencephalography in epilepsy. Ann. Clin. Transl. Neurol. https://doi.org/10.1002/acn3.50995.